Check for updates

Geophysical Research Letters

RESEARCH LETTER
10.1029/2020GL092249

Key Points:

- Orbital-scale Indian Summer Monsoon precipitation isotope record reconstructs precipitation, moisture source, and transport dynamics
- Indian precipitation isotope proxies are quantitatively coherent and show a consistent response to greenhouse gas and ice volume forcing
- Orbital scale Indian and East Asian monsoon precipitation isotopes are uncoupled, responding differently to internal and external forcings

Supporting Information:

- Supporting Information S1

Correspondence to:
S. McGrath,
sarah_mcgrath@brown.edu

Citation:
McGrath, S. M., Clemens, S. C., Huang, Y., & Yamamoto, M. (2021). Greenhouse gas and ice volume drive Pleistocene Indian Summer Monsoon precipitation isotope variability. *Geophysical Research Letters*, *48*, e2020GL092249. https://doi.org/10.1029/2020GL092249

Received 22 DEC 2020
Accepted 14 JAN 2021

© 2021. American Geophysical Union. All Rights Reserved.

Greenhouse Gas and Ice Volume Drive Pleistocene Indian Summer Monsoon Precipitation Isotope Variability

Sarah M. McGrath[1], Steven C. Clemens[1], Yongsong Huang[1], and Masanobu Yamamoto[2]

[1]Department of Earth, Environmental, and Planetary Sciences, Brown University, Providence, RI, USA, [2]Graduate School of Environmental Earth Science, Hokkaido University, Sapporo, Japan

Abstract Orbital-scale Indian Summer Monsoon variability is often interpreted as a direct response to northern hemisphere summer insolation. Here we present a continuous (0–640 kyr) orbital scale precipitation isotope (δD_{precip}) record using leaf wax δD from the core monsoon zone of India. The δD_{precip} record is quantitatively coherent with, and δD_{precip} minima in phase with, greenhouses gas maxima, and ice volume minima across all orbital bands. The δD_{precip} record is also coherent and in phase with the two existing orbital-scale Indian speleothem $\delta^{18}O$ records, demonstrating a consistent regional response among independent proxies. These findings preclude interpretation of Indian precipitation isotope records as a direct response to northern hemisphere summer insolation. Rather, they dominantly reflect changes in moisture source and transport paths associated with changes in greenhouse gases and ice volume. The orbital-scale precipitation isotope responses of the Indian and East Asian monsoon systems are uncoupled and are driven by different forcings.

Plain Language Summary Understanding the variability and forcing mechanisms of the Indian Summer Monsoon is a key socioeconomic concern. Late Pleistocene orbital-scale proxy records provide a unique opportunity to study monsoonal change since both external (insolation) and internal climate forcing functions (greenhouse gases and high-latitude ice volume) are well constrained. Here we present the first long, continuous orbital-scale precipitation isotope proxy record using leaf wax hydrogen isotopes. Precipitation isotopes reflect precipitation amount, moisture source, and moisture transport path dynamics making them ideal proxies for summer monsoon variability. We document a regionally consistent precipitation isotope signal driven by changes in greenhouse gas and ice volume. This diverges from previous studies that interpret the orbital-scale precipitation isotope signal as a direct response to external insolation forcing. Our findings are consistent with model results showing that anthropogenic increases in greenhouse gas will alter large-scale Indian Summer Monsoon circulation leading to increased precipitation and more distal moisture sources.

1. Introduction

Indian Summer Monsoon (ISM) variability is consequential, leading to flooding or droughts, and is tied to the socio-economic stability of India (Gadgil & Gadgil, 2006). Projecting changes in the ISM is a key challenge for global and regional circulation models (e.g., Asharaf & Ahrens, 2015; Seth et al., 2019; Shukla, 2007; Wang et al., 2015), particularly under future climate change scenarios. Orbital-scale proxy records over the Late Pleistocene provide a unique opportunity to study monsoonal change in which the external forcing function, insolation, is known (Berger, 1978; Laskar et al., 2004), and two of the critical internal forcing functions, greenhouse gases and terrestrial ice volume, are well constrained from ice core and benthic foraminifera $\delta^{18}O$ records respectively (Bereiter et al., 2015; Lisiecki & Raymo, 2005; Loulergue et al., 2008). The relative sensitivity of monsoonal proxy records to these external and internal drivers can be evaluated using cross-spectral analysis, a means of quantifying coherence and phase relationships among them.

Previous orbital-scale studies do not yield consistent interpretations with regard to the timing or causes of ISM variability. The phase of the Arabian Sea proxies suggests that the timing of the strongest summer-monsoon winds is sensitive to latent heat imported from the southern hemisphere, greenhouse gas concentrations, and high-latitude ice volume and sea ice cover (Caley et al., 2011; Clemens & Prell, 2003). Runoff (Gebregiorgis et al., 2020) and wind-driven stratification proxies (Bolton et al., 2013) from the Bay

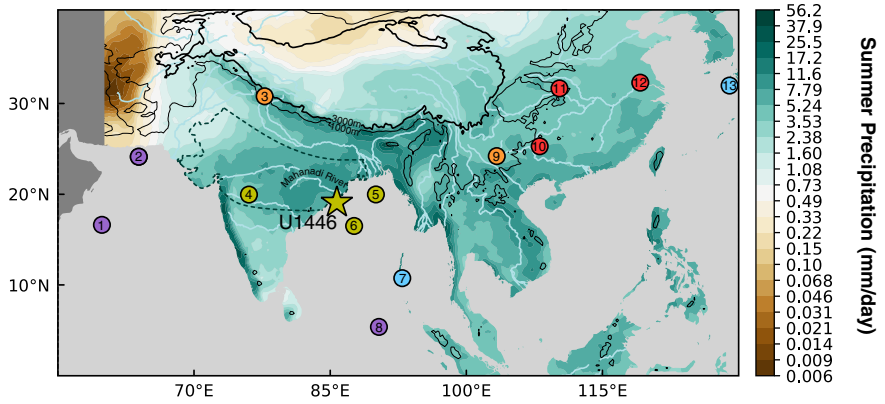

Figure 1. Mean June–September precipitation from APHRODITE (mm day^{-1}; 1998–2015; V1901) (Yatagai et al., 2012) plotted with a logarithmic scale. The dashed line outlines the CMZ of India (Gadgil, 2003) and star marks Site U1446. Dots are color-coded by proxy record type: yellow indicates δD_{wax}, purple indicates wind, orange indicates ISM speleothems, red indicates East Asian summer monsoon speleothems, and blue indicates $\delta^{18}O_{seawater}$. Sites references: (1) RC27-61 and 722B (Clemens & Prell, 2003), (2) MD04-2861 (Caley et al., 2011), (3) Bittoo Cave Speleothem (Kathayat et al., 2016), (4) Lonar Lake (Sarkar et al., 2015), (5) SO188-342 KL (Contreras-Rosales et al., 2014), (6) SO93-117 KL, SO93-118 KL, and SO93-120 KL (Hein et al., 2017), (7) NGHP 17 (Gebregiorgis et al., 2018), (8) Site 758 (Bolton et al., 2013), (9) Xiaobailong Cave (Cai et al., 2015), (10) Dongge Cave (Cheng et al., 2016), (11) Sanbao Cave (Cheng et al., 2016), (12) Hulu Cave (Cheng et al., 2016), and (13) Site U1429 (Clemens et al., 2018).

of Bengal support these internal forcing inferences, providing evidence that ISM winds and precipitation are coupled at precession frequencies. However, both Bay of Bengal wind and runoff records have different obliquity phases compared to the Arabian Sea wind records.

Currently there exists two speleothem $\delta^{18}O$ records of sufficient length (~200,000 years; 200 kyr) to monitor orbital-scale ISM dynamics using time-series analytical approaches. Xiaobailong (XBL) speleothem $\delta^{18}O$ from southwestern China, shows precession and glacial-interglacial variability interpreted to reflect changes in regional ISM precipitation and variable moisture trajectories (Cai et al., 2015). Bittoo speleothem $\delta^{18}O$ from northwestern Indian Himalayan foothills, shows precession variability similar to that in the East Asian speleothem composite (Cheng et al., 2016); interpreted to reflect a consistent Indian and East Asian monsoon precipitation isotope response to northern hemisphere summer insolation forcing (Kathayat et al., 2016). Both XBL and Bittoo precession variability are interpreted as direct responses to northern hemisphere summer insolation forcing.

None of these proxies capture monsoon variability in the core monsoon zone (CMZ) of India, an area that receives significant summer monsoon rainfall and correlates to all-India summer monsoon rainfall (Gadgil, 2003). Here we present the first such proxy record, a precipitation isotope (δD_{precip}) record, based on leaf wax δD (Text S1), spanning the last 640 kyr from International Ocean Discovery Program Site U1446, northwestern Bay of Bengal (Figure 1). We interpret the δD_{precip} variability to reflect ISM circulation; changes in precipitation, moisture source, and moisture transport dynamics. Hence, our use of the term "circulation" refers to the large-scale cross-equatorial overturning circulation of the atmosphere that carries moisture associated with monsoon rainfall.

Quantitative spectral analysis of the variance, coherence, and phase of δD_{precip} relative to existing records clarifies the sensitivity of Indian precipitation isotopes to external and internal climate forcing. The δD_{precip} response across precession and obliquity is consistent with that of the speleothem $\delta^{18}O$ records, all of which are in phase with greenhouse gas radiative forcing maxima and ice volume minima. This indicates large-scale ISM circulation encompassing precipitation, moisture source, and moisture transport changes are driven by the radiative forcing effects of greenhouse gasses and ice volume.

2. Background and Approach

2.1. Site Description

Indian margin Site U1446 (19°5.0'N, 85°44.0'E, 1440 mbsl, 70 km offshore) (Figure 1) is located near the mouth of the Mahanadi catchment (Clemens et al., 2016). The majority of sediment and terrestrial organic matter at Site U1446 comes from the Mahanadi River Basin (Dunlea et al., 2020) (Figure S1). The Mahanadi River Basin receives ~85% of the annual rainfall during the ISM (June–August) (Figure 1, Figure S2, and Text S2). The age model was constructed by mapping of U1446 benthic foraminifera $\delta^{18}O$ (Text S3) to the LR04 stack (Lisiecki & Raymo, 2005) using Analyseries (Paillard et al., 1996). Correlations and tie points are shown in Figure 2 and Table S1.

2.2. Precipitation-Isotope Drivers

Modern interannual precipitation isotopes over India are weakly correlated with the "amount effect": greater precipitation amount leads to lighter precipitation isotopes (Rao et al., 2016). Proximal to Site U1446, GNIP stations (IAEA/WMO, 2019) in Bangladesh indicate that annual weighted precipitation isotopes are weakly correlated with total annual precipitation amount ($r^2 = 0.32$) and annual average water vapor pressure ($r^2 = 0.29$) but have no relationship with annual average temperature ($r^2 = 0.01$) (Figure S3). Hence, the modern precipitation "amount effect" explains about 32% of the total modern variance. Changes in moisture source origin and transport also impact precipitation isotopes (Text S4).

2.3. δD_{wax} Proxy

Long-chain lipid *n*-alkanoic acids are components of waxy coatings on terrestrial plant leaves that are transported by wind and water into the ocean and are preserved in sediments (Sachse et al., 2012). Multiple lines of evidence support interpretation of the hydrogen isotopic composition of these waxy coatings (δD_{wax}) as a proxy for precipitation isotopic composition (δD_{precip}) over the ISM region. Site U1446 collects leaf wax fatty acids predominantly from the proximal Mahanadi River Basin and small coastal catchments (Dunlea et al., 2020), and we infer that δD_{wax} should be representative of Mahanadi basin-integrated δD_{precip}. Catchment studies in the nearby larger Ganges-Brahmaputra catchment finds the exported signal records the basin-integrated δD_{precip} (Galy et al., 2011). Integrating leaf waxes from a large catchment reduces the variability from different vegetation and microclimates, providing clearer climate signals (Douglas et al., 2012). Although residence time could impose a lag in sedimentary systems, even in the much larger floodplain system of the Ganges-Brahmaputra catchment, leaf wax fatty acids have been shown to have short residence times (from 0.015 to 1.2 kyr) (French et al., 2018; Galy & Eglinton, 2011) that do not interfere with the timing of the forcing and response investigated here.

Holocene records support δD_{wax} as an ISM proxy. Two multiproxy studies in the Bay of Bengal fan interpret Ganges-Brahmaputra basin δD_{wax} as a monsoonal precipitation proxy which exhibits similar variability to monsoonal proxies including speleothem $\delta^{18}O$, salinity, vegetation structure, and runoff records (Contreras-Rosales et al., 2014; Hein et al., 2017). Located within the CMZ, Lonar Lake δD_{wax} is interpreted to reflect monsoonal precipitation, moisture source, and moisture transport changes, demonstrating similar variability to local speleothem and vegetation records (Sarkar et al., 2015). Similarly, we use δD_{wax} from Site U1446 to reconstruct late Pleistocene ISM circulation variability within the local Mahanadi River Basin in the CMZ.

3. δD_{wax} and δD_{precip} Records

Hydrogen isotopes of C_{28} *n*-acid (δD_{wax}) were analyzed at ~2 kyr resolution in sediments from Site U1446 over the last 640 kyr (Text S5). δD_{wax} is converted to δD_{precip} using ice volume and vegetation corrections (Text S6). δD_{precip} is heavier by about 95‰ with a nominally increased range of 3‰ (Figure 2a). All climatic interpretations are made from the corrected δD_{precip} record. However, the results and interpretation of the δD record would be the same regardless of whether or not the corrections are incorporated.

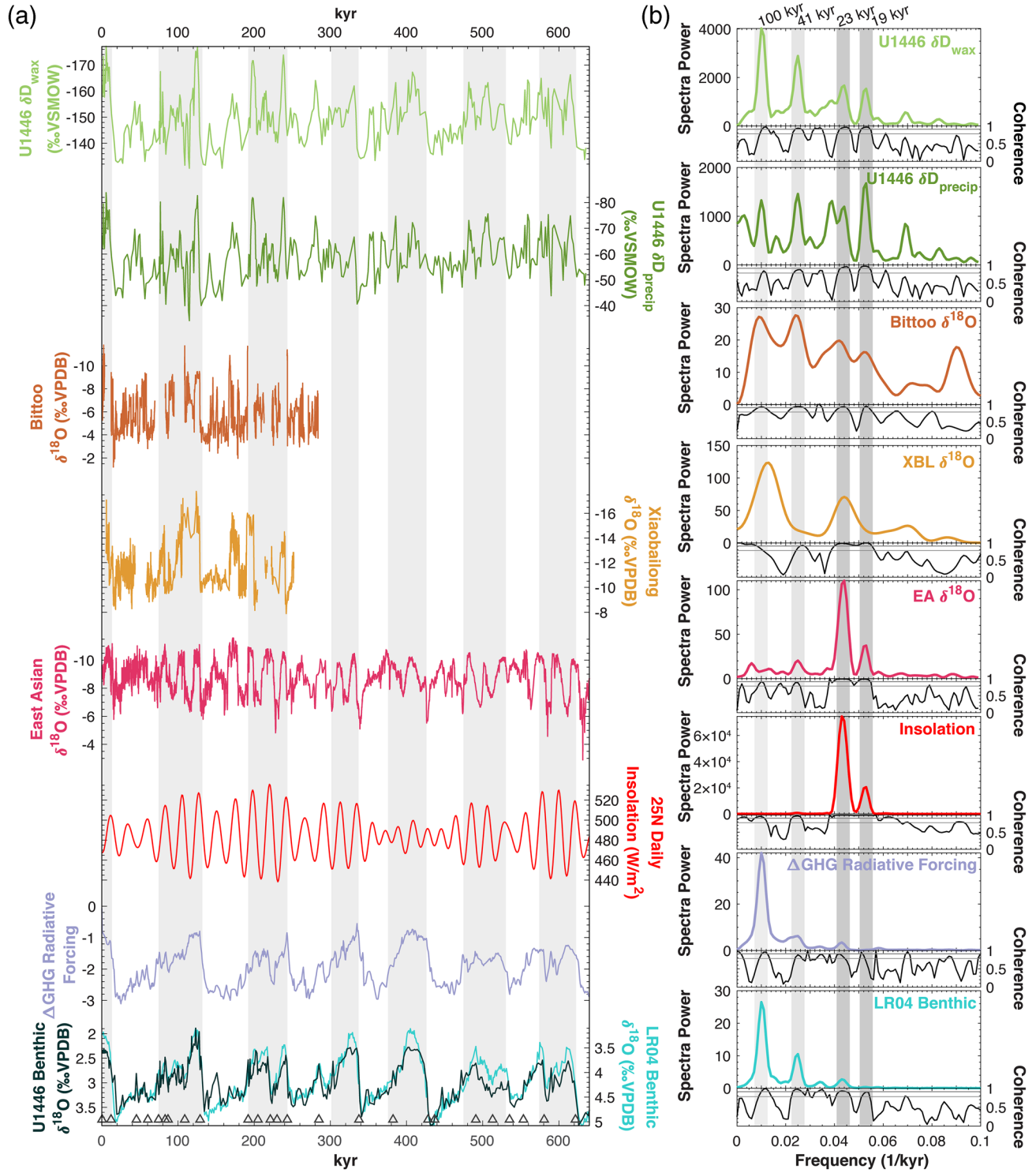

Figure 2. Timeseries and spectra. From top to bottom: U1446 δD_{wax}, U1446 δD_{precip}, Bittoo speleothem $\delta^{18}O$ (Kathayat et al., 2016), Xiaobailong (XBL) speleothem $\delta^{18}O$ (Cai et al., 2015), East Asian (EA) speleothem $\delta^{18}O$ composite (Cheng et al., 2016), daily insolation for June 21 at 25°N (Laskar et al., 2004), radiative forcing of greenhouse gas (Lo et al., 2017) calculated using CO_2 and CH_4 concentration (Bereiter et al., 2015; Loulergue et al., 2008), and the global benthic stack (Lisiecki & Raymo, 2005). (a) Timeseries with light gray bands highlight interglacial periods. At bottom, the U1446 benthic $\delta^{18}O$ stratigraphy overlays the LR04 stack with triangles indicating tie points. (b) Proxy spectra and coherence relative to ETP up to 640kyr or maximum record length with a 50% lag calculated on ARAND software (Howell et al., 2006). For coherence, thin and thick gray lines represent 80% and 95% confidence intervals, respectively. Gray bands highlight eccentricity, obliquity, and precession frequencies.

3.1. Spectral Structure

Both the δD_{wax} and δD_{precip} records show heavier values during glacial periods and lighter values during interglacial periods (Figure 2a). Superimposed on the glacial-interglacial pattern are higher frequency variations driven by precession and obliquity. This is clearly reflected in the spectral analysis of the records relative to ETP, a normalize average record of eccentricity, tilt (obliquity) and precession (June 21 perihelion). δD_{wax} spectral structure is dominated by 100 kyr eccentricity, 41 kyr obliquity, 23 and 19 kyr precession cycles (Figure 2b). δD_{precip} has the same peaks, but with relatively increased 19 kyr precession-band variance due to the vegetation and ice volume corrections lowering the spectral power across eccentricity, obliquity, and precession (23 kyr) frequencies (Figure 2b).

3.2. Coherence and Phase

Coherence provides a measure of linear correlation among variables as a function of frequency while phase indicates the temporal leads and lags critical to understand forcing and response relationships (Tables S1 and S3). δD_{wax} and δD_{precip} are highly coherent with one another (Tables S3) and in phase at the 100 kyr eccentricity, 41 kyr obliquity, and 23 kyr precession cycles (Table S2). The δD_{wax} and δD_{precip} are highly coherent with orbital parameters (eccentricity, obliquity, and precession) (Table S2) as well as with ice volume and greenhouse gas concentration (Tables S3).

4. Discussion

4.1. Consistent Indian Summer Monsoon Precipitation Isotope Signal

The δD_{precip} spectral structure is similar to Indian monsoon speleothem $\delta^{18}O$ spectral structure. Bittoo speleothem $\delta^{18}O$ has variance at the 100- and 41-kyr spectral bands exceeding that at the precession band (Figure 2b). XBL speleothem $\delta^{18}O$ has 100-kyr variance exceeding that at the precession band as well (Figure 2b). Local insolation is dominated by precession variance while internal climate forcings including ice volume and greenhouse gas radiative forcing are all dominated by eccentricity and obliquity variance. The existence of significant of variance at the 100- and 41-kyr spectral bands indicates the ISM precipitation isotopes are strongly sensitive to internal climate drivers, as opposed to direct insolation forcing. Both the speleothem $\delta^{18}O$ and U1446 δD_{precip} records show large-amplitude changes at terminations, further linking variability in these proxies to climate change boundary conditions driven by ice volume and greenhouse gas.

Beyond spectral structure, coherence and phase analysis offer a means of quantifying relationships among time series. At precession, δD_{precip} lags precession minima by about 4.9 kyrs and obliquity maxima by 5.6 kyrs. At both precession and obliquity, δD_{precip} is coherent and in phase with Bittoo speleothem $\delta^{18}O$ as well (Figure 3, Tables S2 and S3). Finally, at precession, δD_{precip} is coherent and in phase with XBL speleothem $\delta^{18}O$ (Figure 3, Tables S2 and S3). These relationships indicate a consistent ISM precipitation isotope response in records recovered from both terrestrial and marine archives, using two independent (organic and inorganic) proxies. δD_{precip} is consistently in phase with ice volume minimum and greenhouse gas maxima at both precession and obliquity (Figure 3, Table S2). In short, $\delta D_{precip,}$ Bittoo and XBL speleothem $\delta^{18}O$ are all coherent with ice volume and greenhouse gas across the orbital frequencies (Table S3). Since Bittoo and XBL are highly coherent with each other, a Bittoo-XBL composite was created, filling in the gaps in Bittoo with XBL (Figure S4). This composite is also highly coherent with both δD_{precip} and the internal climate parameters (Table S3). This multiproxy ISM precipitation isotope response is maximized (lightest values) at times of maximum greenhouse gas radiative forcing and minimum high-latitude ice-volume indicating a common, strong response to internal climate forcings. Below we place these findings in context with other proxies and provide our climatic interpretation.

4.2. Indian Summer Monsoon Proxy Comparison

Beyond the ISM precipitation isotope proxies discussed above, a range of summer monsoon wind and seawater $\delta^{18}O$ records from the Arabian Sea and Bay of Bengal also have significant spectral structure outside of precession, further documenting ISM sensitivity to ice volume and greenhouse gas forcing. However,

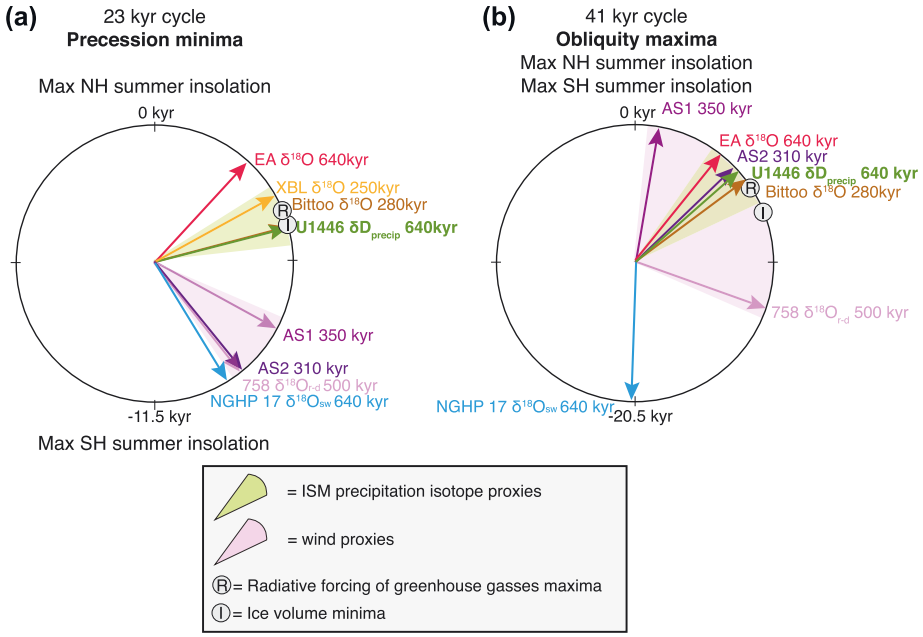

Figure 3. Phase wheels of (a) precession and (b) obliquity ISM records. U1446 δD_{precip}, Bittoo speleothem $\delta^{18}O$ (Kathayat et al., 2016), and XBL speleothem $\delta^{18}O$ (Cai et al., 2015), compared with East Asian speleothem composite (EA $\delta^{18}O$: Cheng et al., 2016), wind proxies (AS2: Caley et al., 2011; AS1: Clemens & Prell, 2003; 758 $\delta^{18}O_{r\text{-}d}$: Bolton et al., 2013), and runoff proxy (NGHP17 $\delta^{18}O_{sw}$: Gebregiorgis et al., 2018). Dots represent greenhouse gasses radiative forcing maxima from CO_2 and CH_4 (Bereiter et al., 2015; Loulergue et al., 2008) calculated by the method from Lo et al. (2017), and ice volume minima (Lisiecki & Raymo, 2005). Negative/positive phases are measured in the clockwise/anticlockwise direction and represent phase lags/leads relative to precession minima or obliquity maxima. Phase errors are reported in Table S2.

these wind and seawater $\delta^{18}O$ proxies significantly lag the three terrestrial precipitation isotope records at precession. At obliquity the wind proxies are widely distributed (Figure 3).

Andaman Sea site NGHP17 seawater $\delta^{18}O$ is interpreted as a salinity indicator, responding to eastern Bay of Bengal rainfall and runoff from the Salween and Irrawaddy catchments to the north (Gebregiorgis et al., 2018). NGHP 17 seawater $\delta^{18}O$ lags δD_{precip} by about 4 kyrs at precession and about 6 kyrs at obliquity (Figures 1 and 3). These phase differences indicate that terrestrial precipitation isotope and seawater isotope records capture different aspects of the monsoon system. Runoff proxies in the Andaman Sea may be delayed in phase relative to North Indian precipitation isotopes due to differences in rainfall on the eastern and western sides of the Bay of Bengal. Additionally, ISM precipitation isotopes are sensitive to moisture source and moisture transport isotopic effects that may not be reflected in Andaman seawater isotopes.

Wind proxies from the Arabian Sea at sites RC27-61, 722B, and MD04-2861 (Caley et al., 2011; Clemens & Prell, 2003) as well as from eastern equatorial Indian site 758 (Bolton et al., 2013) also lag δD_{precip} at the precession band, by about 4 kyrs (Figures 1 and 3). The uniform wind response at precession indicates Arabian Sea and Bay of Bengal winds both strengthen closer to precession maxima than precession minima. At the obliquity band, the Arabian Sea wind records slightly lead or are in phase with the δD_{precip} suggesting potential links to moisture transport. The equatorial eastern Indian Ocean wind record significantly lags, indicating wind strength in the Arabian Sea and Bay of Bengal are uncoupled at obliquity. We look to simulations to help interpret these phase relationships.

4.3. Model Comparison

U1446 δD_{precip} shows strong glacial-interglacial variability with heavier isotopic signatures during glacials and lighter signatures during interglacials, consistent with isotope-enabled simulations for the ISM region (Cai et al., 2015). If the modern precipitation isotope and rainfall amount regression (Figure S3)

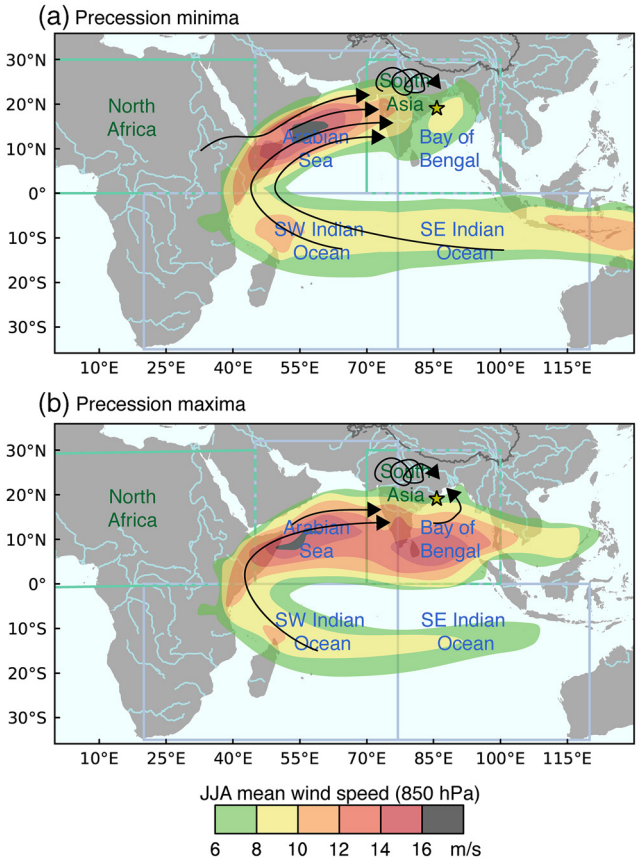

Figure 4. Schematic of precession-band ISM moisture transport. The arrows represent moisture sources from Tabor et al. (2018) and follow the simulated wind field response from Jalihal et al. (2019). The spiral arrow over South Asia represents recycled water from the ISM region. The shading shows June–August mean wind speed (850 hPa) of greater than 6 m/s (after Jalihal et al., 2019). (a) At precession minima, maximum summer wind strength is concentrated in a narrow low-level jet (Jalihal et al., 2019) supporting more distal moisture sources and longer transport paths (Tabor et al., 2018). (b) At precession maxima, maximum summer wind strength is dispersed in a broader low-level jet (Jalihal et al., 2019) supporting more proximal moisture sources and shorter transport paths (Tabor et al., 2018).

is extrapolated back in time, then interglacials were ~30% wetter and glacials ~40% drier compared to modern. A 40% reduction of ISM rainfall during glacial periods aligns with model results indicating precipitation reduction over India between 10% and 50% compared to modern (Chabangborn et al., 2014; Dinezio & Tierney, 2013).

Idealized climate models driven only by insolation show increased ISM precipitation at times of increased summer insolation (minimum precession and maximum obliquity), accompanied by a redistribution of precipitation and convection from ocean to land (Bosmans et al., 2018). Similarly, idealized insolation-only isotope-enabled models show that changes in moisture sources and transport paths also impact precipitation isotopes on orbital timescales (Hu et al., 2019; Tabor et al., 2018), indicating lighter precipitation isotopes in India during high insolation and heavier precipitation isotopes during low insolation (Battisti et al., 2014; Hu et al., 2019; Tabor et al., 2018). However, these models are limited to the equilibrium monsoon responses to orbital forcing only and cannot address phase lags attributed to atmospheric CO_2 and ice volume. These models, as well as time-dependent models that include changes in insolation, ice volume, and greenhouse gas concentration (Caley et al., 2014), all underestimate the isotopic range in both leaf wax δD_{precip} and speleothem $\delta^{18}O_{precip}$ records over India; models indicate about 8‰ change in δD_{precip} (Battisti et al., 2014; Tabor et al., 2018) whereas proxy data indicate about 20‰ change in δD_{precip} at the precession-band time scale.

The δD_{precip} phase relative to runoff proxies suggests that δD_{precip} is capturing a combination of precipitation amount, moisture source, and transport variability. Orbital-scale modeling indicates that moisture source varies as a function of monsoonal circulation, with stronger large-scale circulation leading to lighter precipitation isotopes; due to sourcing from distal regions and longer transport paths (Tabor et al., 2018). At the precession band, two moisture routes are present, feeding into the CMZ of India: a longer path during precession minima and a shorter path during precession maxima (Figure 4). During precession minima, enhanced distal moisture sourcing leads to lighter precipitation isotopes (Tabor et al., 2018) which is supported by a narrow, concentrated low-level jet during precession minima (Jalihal et al., 2019) (Figure 4a). During precession maxima, enhanced proximal moisture sourcing leads to shorter transport distances and heavier precipitation isotopes (Tabor et al., 2018) which is supported by a wider, dispersed low-level jet with stronger Bay of Bengal winds, possibly leading to enhanced (proximal) Bay of Bengal moisture sourcing (Jalihal et al., 2019) (Figure 4b). A similar monsoon circulation pattern is also seen at glacial-interglacial scales with longer moisture transport paths during interglacials, leading to lighter precipitation isotopic values, and shorter moisture transport paths during glacials, leading to heavier precipitation isotopic values (Cai et al., 2015). These models support the interpretation of ISM precipitation isotopes as capturing these large-scale moisture circulation changes.

Additionally, models show there is a difference in the timing of maximum terrestrial versus marine rainfall for the ISM. Increased precipitation over the CMZ at precession minima and increased precipitation over the Bay of Bengal during precession maxima is observed in multiple climate models forced only by insolation (Jalihal et al., 2019; Lee et al., 2019; Tabor et al., 2018). Jalihal et al. (2019) interpret the out-of-phase precipitation over the CMZ and Bay of Bengal as a function of low-level jet dynamics driven by insolation influence on terrestrial precipitation and surface fluxes, and driven by vertical stability influence on precipitation over the ocean. This opposite precession precipitation variability over the India CMZ and Bay of Bengal is reflected in the ~90° phase difference between the Indian δD_{precip} and Andaman Sea seawater $\delta^{18}O$, consistent with the two proxies capturing different components of the monsoon system.

In summary, monsoon proxies are broadly consistent with insolation only model results (which can only yield precipitation and precipitation isotope responses that are in phase with orbital maxima or minima); the proxy δD_{precip} phase falls closer to precession minima while Andaman $\delta^{18}O_{seawater}$ phase falls closer to precession maxima. Neither of the proxy records indicate phase responses aligned with orbital extremes, rather, the phases are drawn away from these orbital positions because of their sensitivity to coupled ice volume and greenhouse gas forcing.

4.4. Interpretation of Indian Versus East Asian Summer Monsoon Records

East Asian speleothem $\delta^{18}O$ records have been used to infer Asian monsoon intensity, grouping together the Indian (South Asian) summer monsoon with the East Asian summer monsoon (e.g., Cheng et al., 2016). East Asian speleothem $\delta^{18}O$ from the Yangtze river valley (YRV) exhibits a dominant precession-band response (Figure 2b) and thus insolation is interpreted as the primary driver of Asian monsoon intensity. This is in contrast to the East China Sea seawater $\delta^{18}O$ record that monitors YRV runoff; having removed the temperature and global ice-volume signals, YRV runoff has little to no precession-band variance (Clemens et al., 2018). As well, isotope enabled climate models suggest that East Asian speleothem $\delta^{18}O$ does not reflect local precipitation amount at the orbital timescale (Battisti et al., 2014; Caley et al., 2014; Hu et al., 2019). Instead, orbital scale East Asian speleothem $\delta^{18}O$ variation is thought to represent large scale dynamics along moisture transport paths (Battisti et al., 2014; Caley et al., 2014; Hu et al., 2019; Zhang et al., 2020).

The spectral structures of U1446 $\delta D_{precip,}$ Bittoo $\delta^{18}O$, and XBL $\delta^{18}O$ records have significant spectral structure outside of precession, unlike the East Asian speleothem $\delta^{18}O$ (Figure 2b). As well, both Bittoo $\delta^{18}O$ and δD_{precip} slightly lag East Asian speleothem $\delta^{18}O$ at precession and obliquity and are in phase with CO_2 maxima and ice volume minima (Figure 3). The spectral structure and phase of U1446 δD_{precip}, Bittoo, and XBL precipitation $\delta^{18}O$ clearly indicate sensitivity to greenhouse gas radiative forcing and ice volume, a finding very different from that based on the East Asian speleothem $\delta^{18}O$ record. On the basis of the difference in spectral structure, coherence, and phase relationships demonstrated here, the precipitation isotope responses of the Indian and East Asian subsystems are uncoupled, responding in different ways to internal and external driving mechanisms at orbital time scales.

5. Conclusions

The ISM δD_{precip} and speleothem $\delta^{18}O$ signals exhibit strong spectral structure outside of precession, show strong glacial-interglacial changes, and are coherent and in phase with greenhouse gas maxima and ice volume minima. This indicates large-scale ISM circulation encompassing precipitation, moisture source, and moisture transport changes are dominated by these internal climate drivers. Proxy phase responses are broadly consistent with insolation-only model experiments showing increased precipitation, more distal moisture sources and longer transport paths leading to lighter isotopes at precession minima and interglacials (Bosmans et al., 2018; Cai et al., 2015; Jalihal et al., 2019; Tabor et al., 2018). On the basis of our results indicating strong sensitivity to CO_2 maxima and ice volume minima, future anthropogenic increases in greenhouse gas radiative forcing may change large-scale ISM circulation leading to increased precipitation and more distal moisture sources.

Data Availability Statement

The U1446 δD_{wax}, δD_{precip}, $\delta^{13}C_{wax,}$ and benthic $\delta^{18}O$ data presented in this study are archived at NOAA's National Centers for Environmental Information (https://www.ncdc.noaa.gov/paleo/study/32374). Supporting paleoclimate datasets are available in these in-text data citation references: Bittoo speleothem $\delta^{18}O$ (Kathayat et al., 2016), Xiaobailong speleothem $\delta^{18}O$ (Cai et al., 2015), East Asian speleothem $\delta^{18}O$ composite (Cheng et al., 2016), wind proxies (AS2: Caley et al., 2011; AS1: Clemens & Prell, 2003; 758 $\delta^{18}O_{r\text{-}d}$: Bolton et al., 2013), runoff proxy (NGHP17 $\delta^{18}O_{sw}$: Gebregiorgis et al., 2018), daily insolation for June 21 at 25°N (Laskar et al., 2004), radiative forcing of greenhouse gas (Lo et al., 2017) calculated using CO_2 and

CH_4 concentration (Bereiter et al., 2015; Loulergue et al., 2008), and the global benthic stack (Lisiecki & Raymo, 2005). The authors declare no conflicts of interest.

Acknowledgments
This research used samples provided by the Integrated Ocean Drilling Program (IODP). This research was supported by NSF Grant #1634774 to S. Clemens and Y. Huang and JSPS grant JPMX-S05R2900001 to M. Yamamoto. We are grateful for the lab support provided by Marcelo Alexandre, Ewerton Santos, and Yuko Tsuchiya. We thank the scientists and ship's crew of IODP Exp 353.

References

Asharaf, S., & Ahrens, B. (2015). Indian summer monsoon rainfall processes in climate change scenarios. *Journal of Climate*, *28*(13), 5414–5429. https://doi.org/10.1175/JCLI-D-14-00233.1

Battisti, D. S., Ding, Q., & Roe, G. H. (2014). Coherent pan-Asian climatic and isotopic response to orbital forcing of tropical insolation. *Journal of Geophysical Research: Atmospheres*, *119*(21), 11997–12020. https://doi.org/10.1002/2014JD021960

Bereiter, B., Eggleston, S., Schmitt, J., Nehrbass-Ahles, C., Stocker, T. F., Fischer, H., et al. (2015). Revision of the EPICA Dome C CO_2 record from 800 to 600 kyr before present. *Geophysical Research Letters*, *42*(2), 542–549. https://doi.org/10.1002/2014GL061957

Berger, A. L. (1978). Long-term variations of caloric insolation resulting from the Earth's orbital elements. *Quaternary Research*, *9*(02), 139–167. https://doi.org/10.1016/0033-5894(78)90064-9

Bolton, C. T., Chang, L., Clemens, S. C., Kodama, K., Ikehara, M., Medina-Elizalde, M., et al. (2013). A 500,000-year record of Indian summer monsoon dynamics recorded by eastern equatorial Indian Ocean upper water-column structure. *Quaternary Science Reviews*, *77*, 167–180. https://doi.org/10.1016/j.quascirev.2013.07.031

Bosmans, J. H. C., Erb, M. P., Dolan, A. M., Drijfhout, S. S., Tuenter, E., Hilgen, F. J., et al. (2018). Response of the Asian summer monsoons to idealized precession and obliquity forcing in a set of GCMs. *Quaternary Science Reviews*, *188*, 121–135. https://doi.org/10.1016/j.quascirev.2018.03.025

Cai, Y., Fung, I. Y., Edwards, R. L., An, Z., Cheng, H., Lee, J. E., et al. (2015). Variability of stalagmite-inferred Indian monsoon precipitation over the past 252,000 y. *Proceedings of the National Academy of Sciences of the United States of America*, *112*(10), 2954–2959. https://doi.org/10.1073/pnas.1424035112

Caley, T., Malaizé, B., Zaragosi, S., Rossignol, L., Bourget, J., Eynaud, F., et al. (2011). New Arabian Sea records help decipher orbital timing of Indo-Asian monsoon. *Earth and Planetary Science Letters*, *308*(3–4), 433–444. https://doi.org/10.1016/J.EPSL.2011.06.019

Caley, T., Roche, D. M., & Renssen, H. (2014). Orbital Asian summer monsoon dynamics revealed using an isotope-enabled global climate model. *Nature Communications*, *5*(1), 5371. https://doi.org/10.1038/ncomms6371

Chabangborn, A., Brandefelt, J., & Wohlfarth, B. (2014). Asian monsoon climate during the Last Glacial Maximum: paleo-data-model comparisons. *Boreas*, *43*(1), 220–242. https://doi.org/10.1111/bor.12032

Cheng, H., Edwards, R. L., Sinha, A., Spötl, C., Yi, L., Chen, S., et al. (2016). The Asian monsoon over the past 640,000 years and ice age terminations. *Nature*, *534*(7609), 640–646. https://doi.org/10.1038/nature18591

Clemens, S. C., Holbourn, A., Kubota, Y., Lee, K. E., Liu, Z., Chen, G., et al. (2018). Precession-band variance missing from East Asian monsoon runoff. *Nature Communications*, *9*(1), 3364. https://doi.org/10.1038/s41467-018-05814-0

Clemens, S. C., Kuhnt, W., LeVay, L. J., & Expedition 353 Scientists (2016). Site U1446. *Proceedings of the International Ocean Discovery Program* (Vol. *353*). https://doi.org/10.14379/iodp.proc.353.106.2016

Clemens, S. C., & Prell, W. L. (2003). A 350,000-year summer-monsoon multi-proxy stack from the Owen Ridge, Northern Arabian Sea. *Marine Geology*, *201*(1–3), 35–51. https://doi.org/10.1016/S0025-3227(03)00207-X

Contreras-Rosales, L. A., Jennerjahn, T., Tharammal, T., Meyer, V., Lückge, A., Paul, A., & Schefuß, E. (2014). Evolution of the Indian Summer Monsoon and terrestrial vegetation in the Bengal region during the past 18 ka. *Quaternary Science Reviews*, *102*, 133–148. https://doi.org/10.1016/J.QUASCIREV.2014.08.010

Dinezio, P. N., & Tierney, J. E. (2013). The effect of sea level on glacial Indo-Pacific climate. *Nature Geoscience*, *6*(6), 485–491. https://doi.org/10.1038/ngeo1823

Douglas, P. M. J., Pagani, M., Brenner, M., Hodell, D. A., & Curtis, J. H. (2012). Aridity and vegetation composition are important determinants of leaf-wax δD values in southeastern Mexico and Central America. *Geochimica et Cosmochimica Acta*, *97*, 24–45. https://doi.org/10.1016/j.gca.2012.09.005

Dunlea, A., Giosan, L., & Huang, Y. (2020). Pliocene expansion of C4 vegetation in the core monsoon zone on the Indian Peninsula. *Climate of the Past*, *16*, 2533–2546. https://doi.org/10.5194/cp-16-2533-2020

French, K. L., Hein, C. J., Haghipour, N., Wacker, L., Kudrass, H. R., Eglinton, T. I., & Galy, V. (2018). Millennial soil retention of terrestrial organic matter deposited in the Bengal Fan. *Scientific Reports*, *8*(1), 1197. https://doi.org/10.1038/s41598-018-30091-8

Gadgil, S. (2003). The Indian monsoon and its variability. *Annual Review of Earth and Planetary Sciences*, *31*(1), 429–467. https://doi.org/10.1146/annurev.earth.31.100901.141251

Gadgil, S., & Gadgil, S. (2006). The Indian monsoon, GDP and agriculture. *Economic and Political Weekly*, *41*(47), 4887–4895. https://doi.org/10.2307/4418949

Galy, V., & Eglinton, T. (2011). Protracted storage of biospheric carbon in the Ganges–Brahmaputra basin. *Nature Geoscience*, *4*(12), 843–847. https://doi.org/10.1038/ngeo1293

Galy, V., Eglinton, T., France-Lanord, C., & Sylva, S. (2011). The provenance of vegetation and environmental signatures encoded in vascular plant biomarkers carried by the Ganges-Brahmaputra rivers. *Earth and Planetary Science Letters*, *304*(1–2), 1–12. https://doi.org/10.1016/j.epsl.2011.02.003

Gebregiorgis, D., Clemens, S., Hathorne, E., Giosan, L., Thirumalai, K., & Frank, M. (2020). A brief commentary on the interpretation of Chinese speleothem $\delta^{18}O$ records as summer monsoon intensity tracers. *Quaternary*, *3*(1), 7. https://doi.org/10.3390/quat3010007

Gebregiorgis, D., Hathorne, E. C., Giosan, L., Clemens, S., Nürnberg, D., & Frank, M. (2018). Southern Hemisphere forcing of South Asian monsoon precipitation over the past ~1 million years. *Nature Communications*, *9*(1), 4702. https://doi.org/10.1038/s41467-018-07076-2

Hein, C. J., Galy, V., Galy, A., France-Lanord, C., Kudrass, H., & Schwenk, T. (2017). Post-glacial climate forcing of surface processes in the Ganges–Brahmaputra river basin and implications for carbon sequestration. *Earth and Planetary Science Letters*, *478*, 89–101. https://doi.org/10.1016/J.EPSL.2017.08.013

Howell, P., Pisias, N., Ballance, J., Baughman, J., & Ochs, L. (2006). *ARAND time-series analysis software*. Providence, RI: Brown University.

Hu, J., Emile-Geay, J., Tabor, C., Nusbaumer, J., & Partin, J. (2019). Deciphering oxygen isotope records from chinese speleothems with an isotope-enabled climate model. *Paleoceanography and Paleoclimatology*, *34*, 2098–2112. https://doi.org/10.1029/2019PA003741

IAEA/WMO (2019). *Global network of isotopes in precipitation*. The GNIP Database. Retrieved from https://nucleus.iaea.org/wiser

Jalihal, C., Helena Catharina Bosmans, J., Srinivasan, J., & Chakraborty, A. (2019). The response of tropical precipitation to Earth's precession: the role of energy fluxes and vertical stability. *Climate of the Past*, *15*, 449–462. https://doi.org/10.5194/cp-15-449-2019

Kathayat, G., Cheng, H., Sinha, A., Spötl, C., Edwards, R. L., Zhang, H., et al. (2016). Indian monsoon variability on millennial-orbital timescales. *Scientific Reports*, *6*(1), 24374. https://doi.org/10.1038/srep24374

Laskar, J., Robutel, P., Joutel, F., Gastineau, M., Correria, A. C. M., & Levrard, B. (2004). A long-term numerical solution for the insolation quantities of the Earth. *Astronomy and Astrophysics*, *428*, 261–285. https://doi.org/10.1051/0004-6361:20041335

Lee, J., Fox-Kemper, B., Horvat, C., & Ming, Y. (2019). The response of East Asian monsoon to the precessional cycle: A new study using the Geophysical Fluid Dynamics Laboratory model. *Geophysical Research Letters*, *46*, 11388–11396. https://doi.org/10.1029/2019gl082661

Lisiecki, L. E., & Raymo, M. E. (2005). A Pliocene-Pleistocene stack of 57 globally distributed benthic δ18O records. *Paleoceanography*, *20*(1), 1–17. https://doi.org/10.1029/2004PA001071

Lo, L., Chang, S. P., Wei, K. Y., Lee, S. Y., Ou, T. H., Chen, Y. C., et al. (2017). Nonlinear climatic sensitivity to greenhouse gases over past 4 glacial/interglacial cycles. *Scientific Reports*, *7*(1), 1–7. https://doi.org/10.1038/s41598-017-04031-x

Loulergue, L., Schilt, A., Spahni, R., Masson-Delmotte, V., Blunier, T., Lemieux, B., et al. (2008). Orbital and millennial-scale features of atmospheric CH_4 over the past 800,000 years. *Nature*, *453*(7193), 383–386. https://doi.org/10.1038/nature06950

Paillard, D., Labeyrie, L., & Yiou, P. (1996). Macintosh Program performs time-series analysis. *Eos, Transactions American Geophysical Union*, *77*(39), 379. https://doi.org/10.1029/96EO00259

Rao, Z., Li, Y., Zhang, J., Jia, G., & Chen, F. (2016). Investigating the long-term palaeoclimatic controls on the δD and $\delta^{18}O$ of precipitation during the Holocene in the Indian and East Asian monsoonal regions. *Earth-Science Reviews*, *159*, 292–305. https://doi.org/10.1016/J.EARSCIREV.2016.06.007

Sachse, D., Billault, I., Bowen, G. J., Chikaraishi, Y., Dawson, T. E., Feakins, S. J., et al. (2012). Molecular paleohydrology: Interpreting the hydrogen-isotopic composition of lipid biomarkers from photosynthesizing organisms. *Annual Review of Earth and Planetary Sciences*, *40*(1), 221–249. https://doi.org/10.1146/annurev-earth-042711-105535

Sarkar, S., Prasad, S., Wilkes, H., Riedel, N., Stebich, M., Basavaiah, N., & Sachse, D. (2015). Monsoon source shifts during the drying mid-Holocene: Biomarker isotope based evidence from the core "monsoon zone" (CMZ) of India. *Quaternary Science Reviews*, *123*, 144–157. https://doi.org/10.1016/j.quascirev.2015.06.020

Seth, A., Giannini, A., Rojas, M., Rauscher, S. A., Bordoni, S., Singh, D., & Camargo, S. J. (2019). Monsoon responses to climate changes—Connecting past, present and future. *Current Climate Change Reports*, *5*(2), 63–79. https://doi.org/10.1007/s40641-019-00125-y

Shukla, J. (2007). Monsoon mysteries. *Science*, *318*(5848), 204–205. https://doi.org/10.1126/science.1150045

Tabor, C. R., Otto-Bliesner, B. L., Brady, E. C., Nusbaumer, J., Zhu, J., Erb, M. P., et al. (2018). Interpreting precession-driven $\delta^{18}O$ variability in the south Asian monsoon region. *Journal of Geophysical Research: Atmospheres*, *123*(11), 5927–5946. https://doi.org/10.1029/2018JD028424

Wang, B., Xiang, B., Li, J., Webster, P. J., Rajeevan, M. N., Liu, J., & Ha, K. J. (2015). Rethinking Indian monsoon rainfall prediction in the context of recent global warming. *Nature Communications*, *6*(1), 7154. https://doi.org/10.1038/ncomms8154

Yatagai, A., Kamiguchi, K., Arakawa, O., Hamada, A., Yasutomi, N., & Kitoh, A. (2012). Aphrodite constructing a long-term daily gridded precipitation dataset for Asia based on a dense network of rain gauges. *Bulletin of the American Meteorological Society*, *93*(9), 1401–1415. https://doi.org/10.1175/BAMS-D-11-00122.1

Zhang, H., Cheng, H., Baker, J., & Kathayat, G. (2020). Response to comments by Daniel Gebregiorgis et al. "A brief commentary on the interpretation of Chinese speleothem $\delta^{18}O$ records as summer monsoon intensity tracers". *Quaternary*, 3, 7. *Quaternary*, *3*(1), 8. https://doi.org/10.3390/quat3010008

References From the Supporting Information

Ansari, M. A., Noble, J., Deodhar, A., & Saravana Kumar, U. (2020). Atmospheric factors controlling the stable isotopes ($\delta^{18}O$ and $\delta^{2}H$) of the Indian summer monsoon precipitation in a drying region of Eastern India. *Journal of Hydrology*, *584*, 124636. https://doi.org/10.1016/j.jhydrol.2020.124636

Breitenbach, S. F. M., Adkins, J. F., Meyer, H., Marwan, N., Kumar, K. K., & Haug, G. H. (2010). Strong influence of water vapor source dynamics on stable isotopes in precipitation observed in Southern Meghalaya, NE India. *Earth and Planetary Science Letters*, *292*(1–2), 212–220. https://doi.org/10.1016/j.epsl.2010.01.038

Giosan, L., Ponton, C., Usman, M., Blusztajn, J., Fuller, D. Q., Galy, V., et al. (2017). Massive erosion in monsoonal central India linked to late Holocene land cover degradation. *Earth Surface Dynamics*, *5*(4), 781–789. https://doi.org/10.5194/esurf-5-781-2017

Hurley, J. V., & Boos, W. R. (2015). A global climatology of monsoon low-pressure systems. *Quarterly Journal of the Royal Meteorological Society*, *141*(689), 1049–1064. https://doi.org/10.1002/qj.2447

Konecky, B., Russell, J., & Bijaksana, S. (2016). Glacial aridity in central Indonesia coeval with intensified monsoon circulation. *Earth and Planetary Science Letters*, *437*, 15–24. https://doi.org/10.1016/j.epsl.2015.12.037

Kumar, B., Rai, S. P., Kumar, U. S., Verma, S. K., Garg, P., Kumar, S. V. V., et al. (2010). Isotopic characteristics of Indian precipitation. *Water Resources Research*, *46*(12), W12548. https://doi.org/10.1029/2009WR008532

Pathak, A., Ghosh, S., Alejandro Martinez, J., Dominguez, F., & Kumar, P. (2017). Role of oceanic and land moisture sources and transport in the seasonal and interannual variability of summer monsoon in India. *Journal of Climate*, *30*(5), 1839–1859. https://doi.org/10.1175/JCLI-D-16-0156.1

Roy, P. S., Behera, M. D., Murthy, M. S. R., Roy, A., Singh, S., Kushwaha, S. P. S., et al. (2015). New vegetation type map of India prepared using satellite remote sensing: Comparison with global vegetation maps and utilities. *International Journal of Applied Earth Observation and Geoinformation*, *39*, 142–159. https://doi.org/10.1016/j.jag.2015.03.003

Ryan, W. B. F., Carbotte, S. M., Coplan, J., O'Hara, S., Melkonian, A., Arko, R., et al. (2009). Global Multi-Resolution Topography (GMRT) synthesis data set. *Geochemistry, Geophysics, Geosystems*, *10*, Q03014. https://doi.org/10.1029/2008GC002332

Schrag, D. P., Hampt, G., & Murray, D. W. (1996). Pore fluid constraints on the temperature and oxygen isotopic composition of the Glacial Ocean. *Science*, *272*(5270), 1930–1932. https://doi.org/10.1126/science.272.5270.1930

Yoon, J.-H., & Chen, T.-C. (2005). Water vapor budget of the Indian monsoon depression. *Tellus A: Dynamic Meteorology and Oceanography*, *57*(5), 770–782. https://doi.org/10.3402/tellusa.v57i5.14737

Zorzi, C., Sanchez Goñi, M. F., Anupama, K., Prasad, S., Hanquiez, V., Johnson, J., & Giosan, L. (2015). Indian monsoon variations during three contrasting climatic periods: The Holocene, Heinrich Stadial 2 and the last interglacial-glacial transition. *Quaternary Science Reviews*, *125*, 50–60. https://doi.org/10.1016/j.quascirev.2015.06.009